Full Paper

Properties and suspension stability of dendronized iron oxide nanoparticles for MRI applications

B. Basly[a], D. Felder-Flesch[a], P. Perriat[b], G. Pourroy[a] and S. Bégin-Colin[a]*

Functionalized iron oxide nanoparticles have attracted an increasing interest in the last 10 years as contrast agents for MRI. One challenge is to obtain homogeneous and stable aqueous suspensions of iron oxide nanoparticles without aggregates. Iron oxide nanoparticles with sizes around 10 nm were synthesized by two methods: the particle size distribution in water suspension of iron oxide nanoparticles synthesized by the co-precipitation method was improved by a process involving two steps of ligand exchange and phase transfer and was compared with that of iron oxide nanoparticles synthesized by thermal decomposition and functionalized by the same dendritic molecule. The saturation magnetization of dendronized nanoparticles synthesized by thermal decomposition was lower than that of nanoparticles synthesized by co-precipitation. The r_2 relaxivity values were shown to decrease with the agglomeration state in suspension and high r_2 values and r_2/r_1 ratios were obtained with nanoparticles synthesized by co-precipitation by comparison with those of commercial products. Dendronized iron oxide nanoparticles thus have potential properties as contrast agent. Copyright © 2010 John Wiley & Sons, Ltd.

Keywords: iron oxide nanoparticle; dendrons; functionalization; organic coating; magnetic properties; suspension stability; particle size distribution; relaxivity measurement

1. Introduction

Superparamagnetic iron oxide nanoparticles (SPION) with appropriate surface coatings (1–6) are widely used for numerous *in vivo* applications such as MRI contrast enhancement (7–10), hyperthermia treatment (11,12), cell sorting (13), drug delivery, immunoassay and tissue repair (14–16). In the biomedical field, most work has been performed to improve the materials' biocompatibility and targeting (17), but only a few investigations and developments have been carried out to improve the quality of the magnetic nanoparticles (NPs), their size distribution and studying the effect of their functionalization on their structural and magnetic properties.

Indeed, high-quality iron oxide NPs with controlled size have to be synthesized as the magnetic properties strongly depend on the nanoparticle size and since biomedical applications require not only high saturation magnetization values but also particle sizes smaller than 100 nm and a narrow particle size distribution in suspension (18–23). The suspension stability depends strongly on the organic coating. Also, recent studies have demonstrated that modification of the surface by an organic coating may influence the final magnetic properties of the functionalized NPs depending on the coupling agent (24–28). Moreover, this coating should ensure biocompatibility and biodistribution and allow targeting specific areas (17,18,23).

For biological applications, dendrimers and especially the so-called 'dendron' building blocks are very promising as the diversity of functionalization brought by the arborescent structure simultaneously solves the problems of biocompatibility, low toxicity, large *in vivo* stability and specificity. Moreover, in addition to the multifunctionalization of a low molecular weight molecule, the arborescent monodisperse building blocks allow a versatility and a control of size (according to the generation) and of physicochemical properties (hydrophilic, lipophilic) (29). The resulting effects on stability (dendrimer effect), contrast qualities, pharmacokinetics and biodistribution of the contrast agents can clearly be identified. We already described dendron anchoring at the surface of NPs synthesized by coprecipitation and showed that such design allows preserving the magnetic properties while minimizing the thickness of the organic shell necessary for a good colloidal stabilization (24,30,31).

Iron oxide nanoparticles have been synthesized by numerous methods (21,32–35) but the most reported and easy one is the co-precipitation method which occurs in water and leads to nanoparticles with sizes in the range 5–40 nm (36,37). However, the NPs are quite aggregated in water suspension after the synthetic step and the direct functionalization does not greatly improve the particle size distribution. Another recent method is the thermal decomposition of iron complex, such as $Fe(CO)_5$, iron oleate and iron acetylacetonate, in high boiling point solvent,

* Correspondence to: S. Bégin-Colin, Institut de Physique et Chimie des Matéri-aux de Strasbourg, UMR CNRS/UDS 7504, 23 rue du Loess BP 43, 67034 Strasbourg Cedex 2, France.
E-mail: sylvie.begin@ipcms.u-strasbg.fr

a B. Basly, D. Felder-Flesch, G. Pourroy, S. Bégin-Colin
Institut de Physique et Chimie des Matériaux de Strasbourg, UMR CNRS/UDS 7504, 23 rue du Loess BP 43, 67034 Strasbourg Cedex 2, France

b P. Perriat
Groupe d'Etudes de Métallurgie Physique et de Physique des Matériaux, UMR 5510 CNRS-INSA de Lyon, F-69621 Villeurbanne Cedex, France
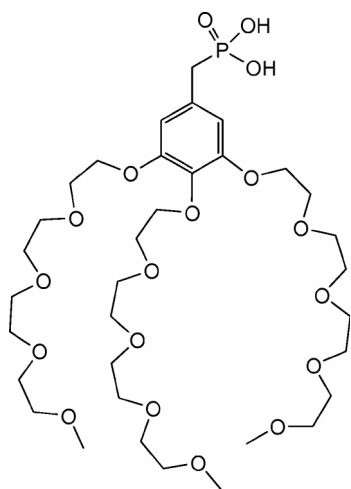
132

Figure 1. Structure of the dendron.

which leads to monodisperse iron oxide nanoparticles coated by fatty acid and forming very stable and monodisperse suspensions in organic solvents (34,38). Water suspensions of these decorated NPs are obtained by a ligand exchange process with a hydrophilic

molecule (21). Moreover NPs synthesized by thermal decomposition are reported to display higher cristallinity and thus higher magnetic properties due to a synthetic process at high temperature (21,39).

In this work, iron oxide NPs were synthesized by co-precipitation (NPcop) and by thermal decomposition of an iron stearate complex (NPtd). Both these NPs are covalently coated with a hydrophilic oligoethyleneglycol-based dendron displaying a phosphonic acid at the focal point (Fig. 1). The suspension stability of the NPcop is improved by a process involving two steps of ligand exchange, and the magnetic properties of all NPs are compared before and after decoration and relaxivity measurement are discussed.

2. Results and discussion

Iron oxide NPs with sizes around 10 nm (Fig. 2) were synthesized by two methods: the co-precipitation of iron chlorides by a base (36) and the thermal decomposition of an iron stearate complex. X-ray and electron diffraction showed that both nanoparticles display the typical spinel structure. The value of the lattice parameter $a = 0.8383$ nm and $a = 0.8384$ nm calculated from XRD patterns for NPcop and NPtd, respectively, is intermediate
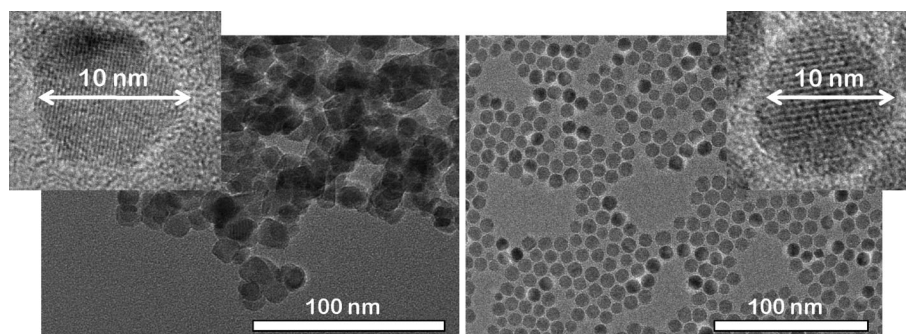

Figure 2. TEM micrographs of iron oxide NPs synthesized by co-precipitation (left) and by thermal decomposition (right).
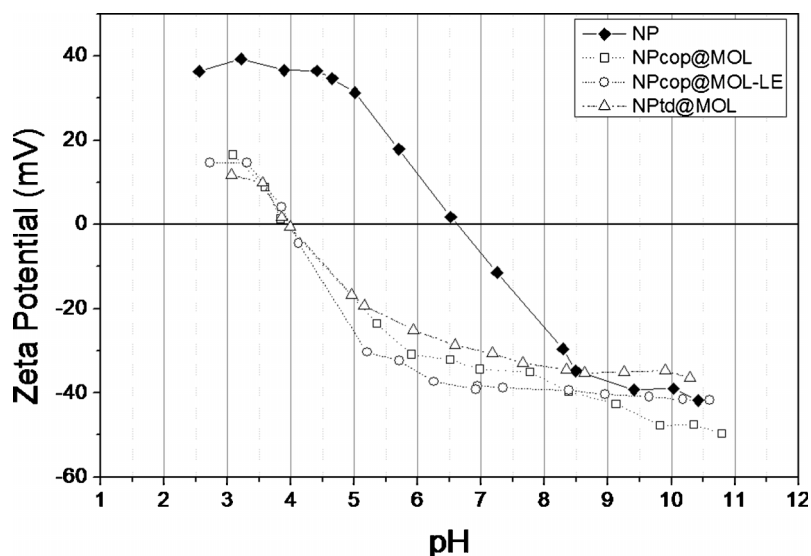

Figure 3. Zeta potential measurements as a function of pH of stripped NPs synthesized by coprecipitation (NPcop), dendronized iron oxide NPs synthesized by co-precipitation and functionalized either directly (NPcop@MOL) or by a two-step process (NPcop@MOL-LE), and of NPs synthesized by thermal decomposition and functionalized by ligand exchange and phase transfer (NPtd@MOL).

between those of magnetite (0.8396 nm, JCPDS file 19-629) and maghemite (0.8346 nm, JCPDS file 39-1346), meaning that the NPs are oxidized at their surface, as already reported for such small sizes (24,31,37,41,42).

After co-precipitation, the stripped iron oxide NPcop is stable in water suspension at pH below 5 or above 7 as the isoelectric point (IEP) of NPcop is 6.8 (Fig. 3). The thermal decomposition method leads to NPs covered with oleic acid in an organic solvent (NPtd). The functionalization step was optimized to obtain stable water suspensions of both iron oxide NPs. For NPcop, the direct grafting by introducing molecules in NPcop water suspensions was demonstrated to occur at pH 5 by interaction of negatively charged phosphonate groups with hydroxyl and positively charged groups at the iron oxide surface (30,31,43). The hydrophilic oligoethyleneglycol-based dendron displaying a phosphonic acid at the focal point was named 'MOL' and the corresponding grafted nanoparticles NPcop@MOL. As observed in Fig. 3, this grafting step induces a shift of the zeta potential curve towards lower pH, leading thus to stable suspensions at physiological pH. The particle size distribution in water of these dendronized NPs is monomodal with an average particle size of about 50 nm (Fig. 4). In order to improve this size distribution, the functionalization process was optimized: the NPcop were first coated with oleic acid and then transferred in hexane (NPcop@AO). The particle size distribution in hexane, given in Fig. 3, presents one peak with an average size of about 28 nm, proving that this first step allows a decrease in the average particle size in suspension. Then, a ligand exchange step with a phase transfer in water was carried out through contact of the NPcop@AO hexane suspension with a water suspension of dendritic phosphonates (NPcop@MOL-LE). After such second step, the particle size distribution was preserved with an average particle size of about 30 nm. The zeta potential curve of these grafted NPs also shifted towards lower pH as observed for the directly grafted NPcop (Fig. 3).

The nanoparticles synthesized by thermal decomposition (NPtd) are coated by oleic acid and form monodisperse and stable suspension in hexane, as observed in Fig. 4. The average particle size is around 13.8 nm, consistent with the diameter of the NPs, taking into account the oleate coating. Then, the organic grafting step also occurs by a ligand exchange and a phase transfer process as for NPcop@OA: the resulting average particle size is slightly increased (30 nm). The same shift of the zeta potential curve to lower pH (Fig. 3) is also observed for these NPtd@MOL, thus confirming the success of this grafting step.

All functionalized NPs (NPcop@MOL, NPcop@MOL-LE and NPtd@MOL) were carefully characterized by XRD, thermogravi-metric analyses (TGA), infra-red spectroscopy, transmission electron microscopy and elemental analyses. Organic coating was also confirmed by IR spectroscopy, showing the disappearance of the P=O and P–OH bands as detailed in Basly *et al*. (30). On the TGA curve recorded for NPcop, only a small weight decrease was observed, resulting from the competition between the oxidation of Fe^{2+} and the loss of adsorbed water. All grafted NPs display a larger weight loss than non-grafted NPs, proving the presence of organic molecules. However, the grafting rate cannot be determined easily by these analyses due to a competitive effect between the weight gain due to the oxidation of Fe^{2+} and the weight loss due to dehydration and decomposition of the dendritic shell. The grafting rate determined by chemical analyses was shown to be similar for all grafted NPs and equal to 1.2, 1.3 and 1.3 molecule/nm^2 for NPcop@MOL,
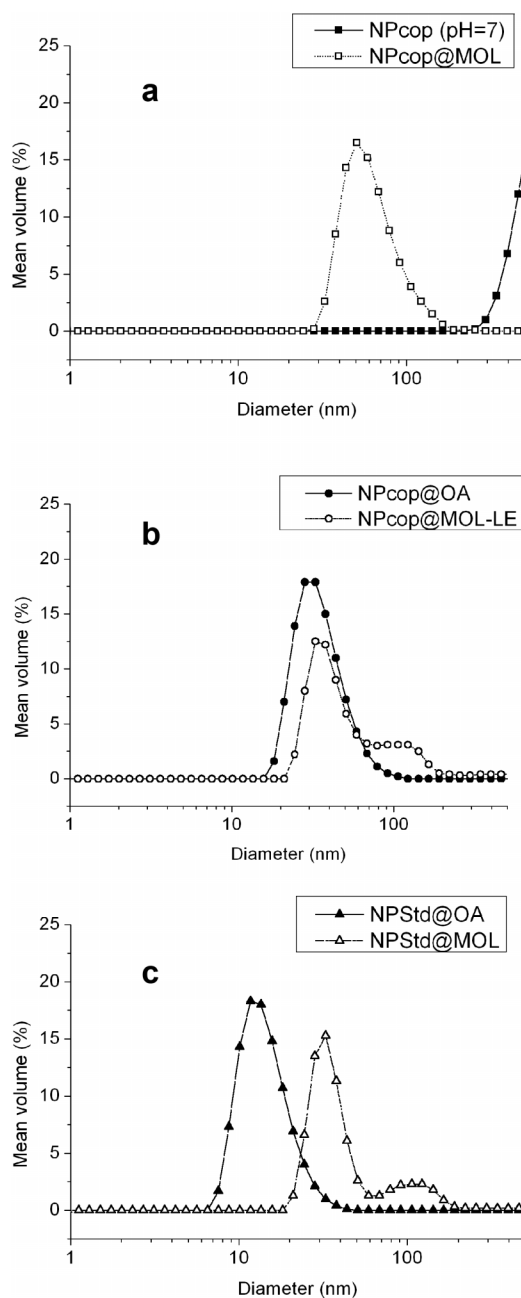

Figure 4. Particle size distribution in water suspension at pH = 6.8 of iron oxide NPs synthesized by co-precipitation before and after direct functionalization (a); after oleic acid coating (NPcop@OA) and after the ligand exchange step (NPcop@MOL-LE) (b); and of NPs synthesized by thermal decomposition before and after the ligand exchange step (c).

NPcop@MOL-LE and NPtd@MOL, respectively, thus very close to the theoretical value of 1.4 molecule/nm^2 for the whole coverage of the NP surface. We calculated this theoretical value by considering that the surface covered by one molecule is equal to 0.75 nm^2 (a value deduced from molecular modeling experiments). The lattice parameters for all functionalized NPs slightly decreased to *ca* 8.375 ± 7 nm, showing that the grafting step induced a slight oxidation of iron oxide NPs.

The magnetization curves of NPs before and after the grafting step are given in Fig. 5. They are all characteristic of super-paramagnetic nanoparticles and demonstrate that the magnetic
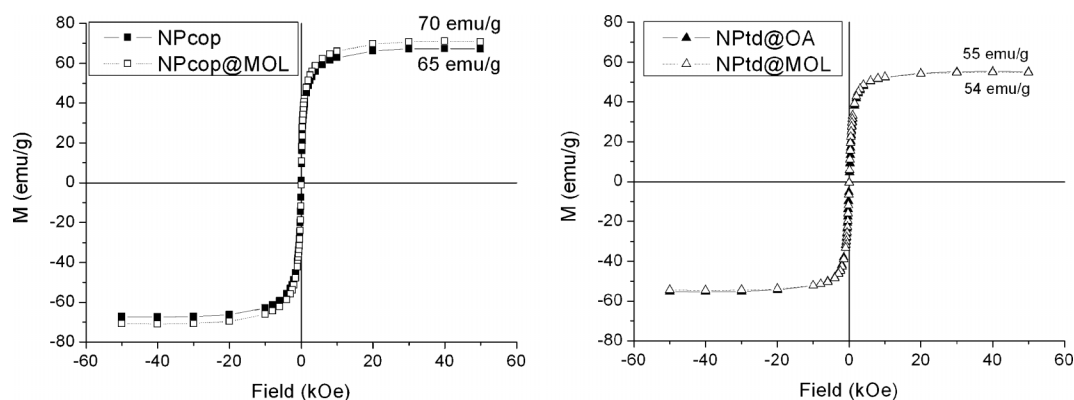
Figure 5. Magnetization curves of NPs synthesized by co-precipitation before and after direct functionalization (left) and of NPs synthesized by thermal decomposition before and after functionalization by ligand exchange and phase transfer (right).

properties of all NPs are preserved after the grafting step. Indeed, the saturation magnetization of the grafted NPcop after subtracting the organic part is about 70 emu/g, a value slightly higher than the one of the starting NPcop (65 emu/g). It is once more demonstrated that phosphonate anchoring preserves the magnetic properties of the iron oxide NPcop, certainly due to super-super exchange interactions through the phosphonate group (24). The magnetic properties of NPtd are also maintained after the grafting step but the saturation magnetizations are observed to be slightly lower than those of NPcop. Further structural investigations are currently underway in our laboratory to explain these different magnetic properties despite the nanoparticle size being the same.

The ZFC/FC curves (Fig. 6) of NPtd before and after grafting are also characteristic of superparamagnetic NPs and the maxima of the ZFC curves may be ascribed to the blocking temperature T_b, which marks the transition from superparamagnetism to ferrimagnetism. The blocking temperature of nanoparticles synthesized by thermal decomposition and coated with oleic acid is around 130 K, consistent with the reported T_b for such size and synthetic method (34,38). After organic coating, a slight shift in T_b is observed, but the ZFC peak is broader with NPtd@OA than with NPtd@MOL, suggesting a distribution of T_b in the NPtd@OA case. This slight shift in T_b towards lower temperature for NPtd@MOL may be attributed either to a modification of the magnetocristalline anisotropy due to the phosphonate grafting

or to weaker dipolar interactions due to the organic coating inducing larger interparticle distances.

The NPs synthesized by coprecipitation display very broad ZFC peaks and the blocking temperature is above 300K (Fig. 6). The aggregation state of NPcop probably induces strong dipolar interactions between NPs and thus a T_b shift towards higher values. When the nanoparticles are coated with the dendritic phosphonates, the ZFC peak maximum is 250 K and, as discussed above, the origin of this shift needs further and deeper characterizations (AC measurements and Mössbauer spectroscopy) to discriminate clearly between surface effect and dipolar interactions. However this shift is consistent with a disaggregation of NPcop after the indirect functionalization process. Indeed one may only underline that, the higher the aggregation state in suspension, the higher the T_b value.

Finally, the relaxation properties of the colloidal suspensions were studied in order to evaluate the possible use of these materials as MRI contrast agents. The effectiveness of contrast agents is usually expressed in term of relaxivities, r_1 and r_2, per millimolar concentration of metal. From *in vitro* relaxivity studies at 1.5 T and at room temperature, values as high as 234 $mm^{-1} s^{-1}$ for r_2, 10 $mm^{-1} s^{-1}$ for r_1, and an r_2/r_1 ratio $\approx$ 25 were obtained for NPcop@MOL with the highest hydrodynamic particle size (Table 1). These values decreased slightly with the particle size, as observed for NPcop@MOL-LE. Such an evolution is consistent with a decrease in the agglomeration state of NPcop (43), but one
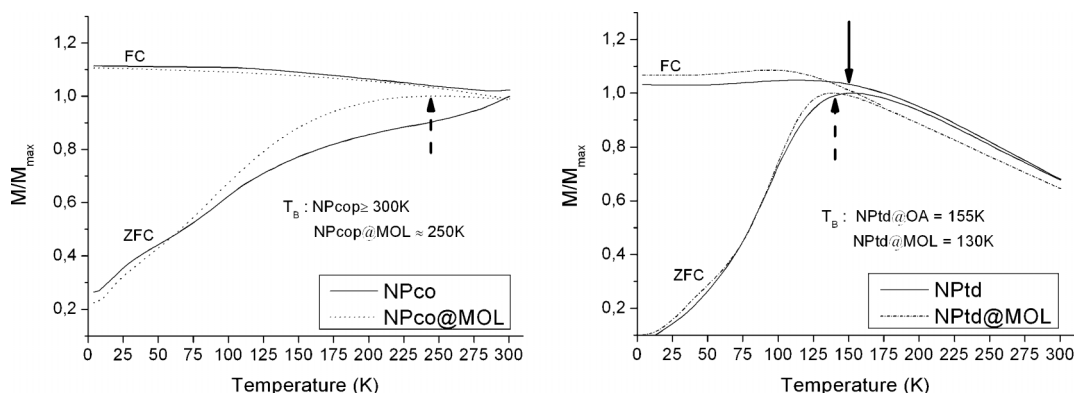

Figure 6. ZFC/FC curves of NPs synthesized by co-precipitation before and after direct functionalization (left) and of NPs synthesized by thermal decomposition before and after functionalization by ligand exchange and phase transfer (right).

Table 1. *In vitro* relaxivity studies (1.5 T, 37 °C) of dendronized NPs compared to some commercial or under clinical investigation products (18)

Name of the compound (company)		Coating agent	Hydrodynamic Size (nm)	r_1 (mM$^{-1} \cdot$s^{-1})	r_2 (mM$^{-1} \cdot$s^{-1})	r_2/r_1
Abdoscan (Ferropharm)		Citrate	7	14	33.4	2.4
Supravist (Schering)		Carboxydextran	21	10.7	38	3.6
Sinerem (Guerbet)		Dextran T10, T1	15–30	9,9	65	6.7
Ferumoxytol (Adv. Magnetics)		Carboxymethyl-dextran T10	30	15	89	5.9
Resovist (Schering)		Carboxydextran	60	9.7	189	19.5
Endorem (Guerbet)		Dextran T10	120–180	10.1	120	11.9
		Our study (Coll. P. Perriat, Lyon)				
Endorem (Guerbet)		Dextran T10	120–180	10.6	141	13.2
Our samples	TD	NPtd@MOL	30	10.4	130	12.5
	COP	NPcop@MOL-LE	30	8.5	160	18.8
		NPcop@MOL	50	10	234	24.9

may notice that both the r_2 value and the r_2/r_1 ratio are among the highest reported for commercial polymer-decorated nanoparticles. Despite similar average hydrodynamic sizes, relaxivity values are lower for NPtd@MOL and may be related to the lower saturation magnetization of these NPs. Nevertheless, one may not conclude clearly on the effect of aggregation for both these powders as the observed T_b shift in ZFC curves may also be the consequence of a modification of the surface properties after the grafting step.

3. Conclusion

Iron oxide nanoparticles with sizes around 10 nm were synthesized by two methods: the co-precipitation of iron chlorides by a base and the thermal decomposition of an iron stearate complex. The NPs synthesized by thermal decomposition were functionalized by a biocompatible dendritic phosphonate through a ligand exchange and phase transfer process. The size distribution in water suspension of NPs synthesized by coprecipitation has been improved by a two-step process involving coating of NPs with oleic acid and then a ligand exchange and phase transfer step. The magnetic properties are essentially preserved after the functionalization step but the saturation magnetization of NPcop was observed to be higher than that of NPtd. All functionalized NPs display high relaxivity values by comparison with commercial polymer-coated nanoparticles. The higher relaxivity value of NPcop obtained through direct functionalization is probably related to their aggregation state and the lower value for functionalized NPtd is mainly related to their lower saturation magnetization. However, further studies dealing with the effect of the grafting step on the surface and magnetic properties (AC measurements) are currently underway. In order to improve the colloidal stability of these dendronized nanoparticles, higher generation dendrons as well as charged dendrons bearing either carboxylic acid or amine groups will be grafted at the surface of nanometer size NPs. Finally, functionalization of the dendron periphery by fluorescent or targeting molecules is also envisaged.

4. Experimental

4.1. Synthesis of NPs

4.1.1. NPcop

Distilled water degassed with argon for half an hour was used for the preparation of 1 M FeCl$_3$·6H$_2$O and 2 M FeCl$_2$·4H$_2$O by dissolving iron salts in 2 M HCl solutions. A 10 ml aliquot of a 1 M FeCl$_3$ solution was mixed with 2.5 ml of a 2 M FeCl$_2$ solution. The so-obtained mixture was stirred and heated up to 70 °C while kept under argon before slow addition of 21 ml of a 25% aqueous solution of N(CH$_3$)$_4$OH. Vigorous stirring was maintained for 20 min. The solution color changed from orange to black, leading to a black precipitate, and the suspension was slowly cooled to room temperature. The powder thus obtained was washed several times by magnetic decantation in water.

4.1.2. NPtd

A 1.38 g (2.22 × 10^{-3} mol) aliquot of Fe(stearate)$_2$ and 1.25 g (4.44 × 10^{-3} mol) of oleic acid (99%, Alfa-Aesar) were added to 20 ml octyl ether (97%, Fluka, b.p. 287 °C). The mixture was kept under vigorous stirring for 1 h to dissolve the reactants. The solution was heated to 287 °C with a heating rate of 5 °C/min without stirring and was refluxed for 120 min at this temperature under air. The resultant black solution was then cooled down to room temperature and the NPs were washed three times by addition of ethanol and by centrifugation (8000 rpm, 10 min). The NPs were then easily suspended in hexane.

4.2. Functionalization process

4.2.1. NPcop

Direct grafting: grafting of dendritic phosphonate in water at the surface of NPcop has been demonstrated to be favored by electrostatic interactions (30,42). Therefore, it must be performed in a pH range determined by the pK_a values of the dendritic phosphonate (3 and 5–6; the pH must be above 3) and by the isoelectric point (IEP) value of bare NPcop, which is 6.8 (pH must be lower than 6.8): thus, the chosen compromise was pH 5 (30). To

achieve this, 50 mg of nanoparticles were added to 40 mg of dendron dissolved in 50 ml of degassed water (pH = 3). Then N(CH₃)₄OH was added in order to reach a pH value of 5. The suspension was sonicated in a standard/laboratory sonicator (Transsonic 275/H Prolabo) for 90 min at 35 °C and the grafted NPs were separated from the ungrafted molecules by ultrafiltration. This technique uses regenerated cellulose membranes with a nominal molecular weight limit (NMWL) of 3 kDa. A 25 ml aliquot of the water suspension was introduced in the apparatus and ultrafiltration (purification) occurred by pressurizing the solution flow. The solvent and ungrafted molecules went through the membrane. The grafted nanoparticles, which did not pass through, were redispersed in 25 ml of water and submitted to another ultrafiltration step. This was done five times. After such purification step, the pH of the NPs suspension was around 6. Such grafted NPs were named NPcop@MOL.

The process involved two ligand exchange steps: 4.9 mg (1.735×10^{-5} mol) of oleic acid (99%, Alfa-Aesar) was added to 5 ml of a water suspension of NPcop (33 mg/ml) at pH = 11. Then pH was adjusted to a value of 3.5 by adding HCl. Oleic acid interacted with the surface of NPcop and, owing to this hydrophobic coating, decorated NPs precipitated and were separated from the water suspension. The black precipitate was washed three times by addition of water and decantation, and three times by addition of ethanol and magnetic decantation. The so-obtained grafted nanoparticles were named NPcop@OA.

The NPcop@OA were transferred in hexane (1 mg/ml) and 10 ml of this suspension was put into contact with a water suspension of the dendritic phosphonate at pH = 4 (13 mg of molecules, 5ml of water and 2 ml of methanol). Both immiscible suspensions were magnetically stirred for one night. A ligand exchange and a phase transfer in water occurred and a water suspension of NPcop was thus obtained. After a purification step by ultrafiltration, the pH of the NPs suspension was around 6. The grafted nanoparticles thus obtained were named NPcop@-MOL-LE.

4.2.2. NPtd

A 10 ml aliquot of a suspension of NPtd@OA in hexane (1 mg/ml) was put into contact with a water suspension of the dendritic phosphonate at pH = 4 (13 mg of molecules, 5 ml of water and 2 ml of methanol). Both immiscible suspensions were magnetically stirred for one night. A ligand exchange and a phase transfer in water occurred and a water suspension of NPtd was thus obtained. After purification steps by ultrafiltration, the pH of the NPs suspension was around 6. The grafted nanoparticles thus obtained were named NPtd@MOL.

4.3. Characterization techniques

The NPs before and after grafting were characterized by X-ray diffraction (XRD) using a Bruker D8 Advance equipped with a monochromatic copper radiation ($K_\alpha = 0.154056$ nm), by transmission electron microscopy with a TOPCON 002B microscope operating at 200 kV (point resolution 0.18 nm) and equipped with a GATAN GIF 200 electron imaging filter.

The grafting step was confirmed by thermogravimetric measurements under air using a TA Instrument apparatus with a heating rate of 5 °C/min and by infra red spectroscopy using a Fourier transform infrared spectrometer (Digilab FTS 3000; samples were gently ground and diluted in non-absorbent KBr matrices).

The grafting rate was determined by chemical analyses. In previous studies, the grafting rate on NPcop was determined indirectly by UV spectroscopy (evaluation of the amount of ungrafted molecules in washing solutions) and directly by chemical analyses of the dendritic hybrids. Both methods gave similar results.

Hysteresis cycles of the NPs and the grafted NPs were recorded at room temperature using a Foner EG&G model 155 vibrating sample magnetometer and ZFC/FC measurements were performed with a Superconducting Quantum Interference Device (Squid) magnetometer (Quantum Design MPMS-XL model) between 5 and 300 K under a field of 75 G.

References

1. Mornet S, Vasseur S, Grasset F, Duguet E. Magnetic nanoparticle design for medical diagnosis and therapy. J Mater Chem 2004; 14: 2161–2175.
2. Lee H, Lee E, Kim DK, Heong YY, Jon S. Antibiofouling polymer-coated superparamagnetic iron oxide nanoparticles as potential magnetic resonance contrast agents for in vivo cancer imaging. J Am Chem Soc 2006; 128: 7383–7389.
3. De M, Ghosh PS, Rotello VM. Applications of nanoparticles in biology. Adv Mater 2008; 20: 4225–4241.
4. Maurizi L, Bisht H, Bouyer F, Millot N. Easy route to functionalize iron oxide nanoparticles via long-term stable thiol groups. Langmuir 2009; 25: 8857–8859.
5. Qiao R, Yang C, Gao M. Superparamagnetic iron oxide nanoparticles: from preparations to in vivo MRI applications. J Mater Chem 2009; 19: 6274–6293.
6. Fang C, Zhang M. Multifunctional magnetic nanoparticles for medical imaging applications. J Mater Chem 2009; 19: 6258–6266.
7. Pankhurst QA, Connolly J, Jones SK, Dobson J. Applications of magnetic nanoparticles in biomedicine. J Phys D: Appl Phys 2003; 36: R167–R181.
8. Lu A-H, Salabas EL, Schüth F. Magnetic nanoparticles: synthesis, protection, functionalization, and application. Angew Chem Int Edn 2007; 46: 1222–1244.
9. Jun Y-W, Lee J-H, Cheon J. Chemical design of nanoparticle probes for high-performance magnetic resonance imaging. Angew Chem Int Edn 2008; 47: 5122–5135.
10. LaConte L, Nitin N, Bao G. Magnetic nanoparticle probes. Mater Today 2005; 8: 32–38.
11. Jordan A, Scholz R, Wust P. Endocytosis of dextran and silan-coated magnetite nanoparticles and the effect of intracellular hyperthermia on human mammary carcinoma cells in vitro. J Magn Magn Mater 1999; 194: 185–196.
12. Ito A, Shinkai M, Honda H, Kobayashi T. Medical application of functionalized magnetic nanoparticles. J Biosci Bioeng 2005; 100: 1–11.
13. Chemla YR, Crossman HL, Poon Y. Ultrasensitive magnetic biosensor for homogeneous immunoassay. Proc Natl Acad Sci USA 2000; 97: 14268–14272.

Copyright © 2010 John Wiley & Sons, Ltd.   wileyonlinelibrary.com/journal/cmmi

14. Liong M, Lu J, Kovochich M, Xia T, Ruehm SG, Nel AE, Tamanoi F, Zink JI. Multifunctional inorganic nanoparticles for imaging, targeting, and drug delivery. ACS Nano 2008; 2: 889–896.

15. McBain SC, Yiu HHP, Dobson J. Magnetic nanoparticles for gene and drug delivery. Int J Nanomed 2008; 3: 169–180.

16. De Jong WH, Borm PJ. Drug delivery and nanoparticles: applications and hazards. Int J Nanomed 2008; 3: 133–149.

17. Berry CC. Progress in functionalization of magnetic nanoparticles for applications in biomedicine. J Phys D: Appl Phys 2009; 42: 224003.

18. Laurent S, Forge D, Port M, Roch A, Robic C, Vander Elst L, Muller RN. Magnetic iron oxide nanoparticles: synthesis, stabilization, vectorization, physicochemical characterizations, and biological applications. Chem Rev 2008; 108: 2064–2110.

19. Forge D, Roch A, Laurent S, Tellez H, Gossuin Y, Renaux F, Vander EL, Muller RN. Optimization of the synthesis of superparamagnetic contrast agents by the design of experiments method. J Phys Chem 2008; 112(49): 19178–19185.

20. Tartaj P, Morales MP, Veintemillas-Verdaguer S, Gonzales-Careno T, Serna C. Advances in magnetic nanoparticles for biotechnology applications. J Magn Magn Mater 2005; 28: 290–291.

21. Roca AG, Costo R, Rebolledo AF, Veintemillas-Verdaguer S, Tartaj P, González-Carreno T, Morales MP, Serna CJ. Progress in the preparation of magnetic nanoparticles for applications in biomedicine. J Phys D: Appl Phys 2009; 42: 224002.

22. Weissleder R, Bogdanov AA, Neuwelt E, Papisov M. Long-circulating iron oxides for MR imaging. Adv Drug Deliv Rev 1995; 16: 321–334.

23. Gupta AK, Gupta M. Synthesis and surface engineering of iron oxide nanoparticles for biomedical applications. Biomaterials 2005; 26: 3995–4021.

24. Daou TJ, Grenèche JM, Pourroy G, Buathong S, Derory A, Ulhaq-Bouillet C, Donnio B, Guillon D, Begin-Colin S. Coupling agent effect on magnetic properties of functionalized magnetite-based nanoparticles. Chem Mater 2008; 20: 5869–5875.

25. Wu W, He QG, Jiang CZ. Magnetic iron oxide nanoparticles: synthesis and surface functionalization strategies. Nano Res Lett 2008; 3: 397–415.

26. Yee C, Kataby G, Ulman A, Prozorov T, White H, King A, Rafailovich M, Sokolov J, Gedanken A. Self-assembled monolayers of alkanesulfonic and phosphonic acids on amorphous iron oxide nanoparticles. Langmuir 1999; 15: 7111–7115.

27. Sahoo Y, Pizem H, Fried T, Golodnitsky D, Burstein L, Sukenik CN, Markovich G. Alkyl phosphonate/phosphate coating on magnetite nanoparticles: a comparison with fatty acids. Langmuir 2001; 17: 7907–7911.

28. Herea DD, Chiriac H. One-step preparation and surface activation of magnetic iron oxide nanoparticles for bio-medical applications. Optoelectron Adv Mater 2008; 2: 549–552.

29. Duncan R, Izzo. L. Dendrimer biocompatibility and toxicity. Adv Drug Deliv Rev 2005; 57: 2215–2237.

30. Basly B, Felder-Flesch D, Perriat P, Billotey C, Taleb J, Pourroy G, Begin-Colin S. Dendronized iron oxide nanoparticles as contrast agent for MRI. Chem Commun 2010; 46: 985–987.

31. Daou TJ, Pourroy G, Greneche JM, Bertin A, Felder-Flesch D, Begin-Colin S. Water soluble dendronized iron oxide nanoparticles. Dalton Trans 2009; 4442–4449.

32. Lu A-H, Salabas EL, Schuth F. Magnetic nanoparticles: synthesis, protection, functionalization, and application. Angew Chem Int Edn 2007; 46: 1222–1244.

33. Jeong U, Teng X, Wang Y, Yang H, Xia Y. Superparamagnetic colloids: controlled synthesis and niche applications. Adv Mater 2007; 19: 33–60.

34. Hyeon T. Chemical synthesis of magnetic nanoparticles. Chem Commun 2003; 927–934.

35. Park J, Lee E, Hwang N-M, Kang M, Kim SC, Hwang Y, Park J-G, Noh H-J, Noh J-Y, Kim J-Y, Park J-H, Hyeon T. One-nanometer-scale size-controlled synthesis of monodisperse magnetic iron oxide nanoparticles. Angew Chem Int Edn 2005; 44: 2872–2877.

36. Massart R. Preparation of aqueous magnetic liquids in alkaline and acidic media. IEEE Trans Magn 1981; 17: 1247–1248.

37. Daou TJ, Begin-Colin S, Greneche JM, Thomas F, Derory A, Bernhardt P, Legaré P, Pourroy G. Hydrothermal synthesis of monodisperse magnetite nanoparticles. Chem Mater 2007; 19: 4494–4505.

38. Park J, An K, Hwang Y, Park J-G, Noh H-J, Kim J-Y, Park J-H, Hwang N-M, Hyeon T. Ultra-large-scale syntheses of monodisperse nanocrystals. Nat Mater 2004; 3: 891–895.

39. Roca AG, Niznansky D, Poltierova-Vejpravova J, Bittova B, González-Fernández MA, Serna CJ, Morales MP. Magnetite nanoparticles with no surface spin canting. J Appl Phys 2009; 105: 114309–114316.

40. Perrat P, Domenichini B, Gillot B. A model for oxidation in finely divided ferrites taking into account the stresses generated during reaction. J Phys Chem Solids 1996; 57: 1641–1652.

41. Guigue-Millot N, Champion Y, Hÿtch M-J, Bernard F, Begin-Colin S, Perriat P. Chemical heterogeneities in nanometric titanomagnetites prepared by soft chemistry and studied ex situ: evidence for fe-segregation and oxidation kinetics. J Phys Chem B 2001; 105: 7125–7132.

42. Daou TJ, Begin-Colin S, Grenèche JM, Thomas F, Derory A, Bernhardt P, Legaré P, Pourroy G. Phosphate adsorption properties of magnetite nanoparticles. Chem Mater 2007; 19: 4494–4505.

43. Roch A, Gossuin Y, Muller RN, Gillis P. Superparamagnetic colloid suspensions: water magnetic relaxation and clustering. J Magn Magn Mater 2005; 293: 532–539.